Published in final edited form as:
Opt Lett. 2003 March 15; 28(6): 414–416.

Dual-axis confocal microscope for high-resolution *in vivo* imaging

Thomas D. Wang,
Stanford University School of Medicine, 269 Campus Drive, Stanford, California 94305-5187

Michael J. Mandella,
Optical Biopsy Technologies, Inc., 235 Alma St., Palo Alto, California 94301

Christopher H. Contag, and
Stanford University School of Medicine, 300 Pasteur Drive, Stanford, California 94305-5208

Gordon S. Kino
Edward L. Ginzton Laboratory, Stanford University, Stanford, California 94305

Abstract

We describe a novel confocal microscope that uses separate low-numerical-aperture objectives with the illumination and collection axes crossed at angle θ from the midline. This architecture collects images in scattering media with high transverse and axial resolution, long working distance, large field of view, and reduced noise from scattered light. We measured transverse and axial (FWHM) resolution of 1.3 and 2.1 μm, respectively, in free space, and confirm subcellular resolution in excised esophageal mucosa. The optics may be scaled to millimeter dimensions and fiber coupled for collection of high-resolution images *in vivo*.

Confocal microscopy provides high-resolution imaging in biological tissue by using the property of optical sectioning.[1] This method is commonly used to collect reflectance and fluorescence images *ex vivo* and potentially can become a powerful tool *in vivo* if the lenses and scanning mechanisms can be made sufficiently small. A transverse resolution of approximately 1–2 μm with comparable axial resolution is adequate for identification of subcellular structures such as cell nucleus and membrane, which are important structures for medical and biological applications. The transverse resolution Δr_s and the axial resolution Δz_s between full width at half-power points for uniform illumination of the lenses are given by the following equations[2]:

$$\Delta r_s = \frac{0.37\lambda}{n \sin \alpha} \approx \frac{0.37\lambda}{n\alpha},$$
$$\Delta z_s = \frac{0.89\lambda}{n(1 - \cos \alpha)} \approx \frac{1.78\lambda}{n\alpha^2}, \quad (1)$$

where λ is the wavelength, n is the refractive index of the medium, α is the maximum convergence angle of the beam, N.A. (=n sin α)is the numerical aperture, and sin $\alpha \approx \alpha$ for low-N.A. lenses.

At present, *in vivo* confocal imaging is limited to exposed tissue surfaces such as skin and oral mucosa[3] because the size of the microscope objective required for achieving high transverse and axial resolution is too large to permit the instrument to be used internally. Equation (1) implies that transverse and axial resolution varies as 1/N.A. and 1/N.A.^{2}, respectively. For an axial resolution of a few micrometers to be achieved, an objective lens must have a large N.A. and a size on a scale of centimeters. The optics cannot be reduced to a millimeter scale without sacrificing resolution, field of view (FOV), or working distance (WD). Also, the scanning mechanism must be located behind the objective, which restricts the FOV and increases sensitivity to aberrations. A microscope reduced in size to millimeter scale can be used to collect *in vivo* confocal images by means of an endoscope in human patients or by implantation in small animals. Previously, a laser scanning confocal microscope was miniaturized with

microelectromechanical system (MEMS) fabrication techniques.[4] This instrument had a single-axis design. It achieved high transverse but poor axial resolution and was not adequately developed for *in vivo* use.

In this Letter we demonstrate the feasibility of a novel dual-axes confocal microscope by predicting and measuring high transverse and axial resolution and long WD. With dual axes,[5,6] two separate low-N.A. lenses are oriented with the illumination and collection axes crossing midline axis z_d at an angle θ, as shown in Fig. 1. First, consider the illumination (IO) and the collection (CO) objectives separately. The main lobe of the point-spread function (PSF) of the illumination objective at the focal point is represented in the figure by a dark gray oval. This lobe has a narrow transverse dimension Δx_s but a wide axial dimension Δz_s. The PSF of the collection objective is similar in shape but symmetrically reflected about z_d, as represented by the light gray oval. For the dual-axes system the combined PSF is the product of the individual PSFs. The intersecting region, represented by the small black oval, is characterized by narrow transverse dimensions, Δx_d and Δy_d (out of the page), and by a significantly reduced axial dimension Δz_d, which depends on the transverse rather than on the axial resolution of the individual beams where they intersect.

To estimate the combined spot size we first transform the optical axes as follows:

$$x_s = x_d \cos\theta \pm z_d \sin\theta, \qquad y_s = y_d. \tag{2}$$

For a low-N.A. lens, the depth of focus in the z_s direction is large; thus the response along and perpendicular to midline axis z_d depends only on Δx_s and not on Δz_s. Combining Eqs. (1) and (2) yields the following transverse ($z_d = 0$) and axial ($x_d = 0$, $y_d = 0$) resolutions for dual axes:

$$\Delta x_d = \frac{0.37\lambda}{na\cos\theta}, \qquad \Delta y_d = \frac{0.37\lambda}{na}, \qquad \Delta z_d = \frac{0.37\lambda}{na\sin\theta}. \tag{3}$$

These results are confirmed by a more-detailed diffraction theory analysis.[7] Thus, with dual axes, low-N.A. lenses can provide an axial resolution (Δz_d) that is proportional to 1/N.A. rather than to 1/N.A.^{2}.

Furthermore, low-N.A. lenses provide a long WD. For a lens with diameter D, the WD is given as follows from geometric arguments:

$$\mathrm{WD} = \frac{D\cos\theta}{2a}. \tag{4}$$

Because the dual-axes beams can achieve an axial resolution of a few micrometers with N.A. of 0.2 or less, lenses with diameters as small as 1 mm can be used to produce a WD of several millimeters. This is sufficient space to allow a MEMS mirror (approximately 300–500 μm) to be placed in front of the objective and to provide beam scanning with the high speeds necessary for *in vivo* imaging. By comparison, conventional high-N.A. oil-immersion objectives have WDs of only approximately 100–200 μm.

To demonstrate proof of principle for a dual-axes system and to check our simple theory of operation, we built the breadboard device shown in Fig. 2, which uses readily available lenses and scans with micrometer stages rather than with a MEMS mirror. The output at 488 nm from a frequency-doubled semiconductor laser (Coherent Sapphire OEM) was passed through a neutral-density filter (ND) and was coupled into a single-mode polarization-maintaining optical fiber (F/O_1) with a mean field diameter of 2.9 μm and a N.A. of 0.11. The polarized light coming out of the fiber was collimated by a 9-mm-diameter axial gradient index lens (L_1), N.A. of 0.15, to a 5-mm-diameter beam and then focused by a 5-mm-diameter aspheric lens (L_2), with a N.A. of 0.16 and a WD of 14.0 mm, to a spot size with a FWHM of 1.22 μm.

The optical axis of illumination was oriented at $\theta = 30°$ to the midline axis. Approximately 400 μW of power was incident upon the scanning stage (*XYZ*). The reflected light was collected and collimated by a microscope objective (O_1; Coherent 24–8690), $f = 14$ mm, N.A. of 0.17, WD of 12.3 mm, and entrance aperture 4.76 mm, which collimated the collected light. A second objective (O_2; Nikon CF Plan EPI SLWD 10×, $f = 20$ mm, N.A. of 0.12, WD of 20.3 mm, entrance aperture 8.4 mm, focused the light into a second single-mode PM fiber (F/O_2) with a mean field diameter of 3.4 μm and N.A. of 0.11. Achromatic objectives were used to accommodate the collection of broadband fluorescence. The output of the collection fiber was connected to a silicon detector. The WD of the complete optical system was measured to be 10.6 mm. Reflectance images were collected at 25 s per frame, digitized, and displayed. The image acquisition time was limited by the maximum speed of the scanning stages.

Figure 3(a) shows the response in free space to a chrome edge taken in the transverse direction with a measured 20–80% edge width of 1.06 μm. The edge response may be estimated by integration of the PSF.[2] This process yields an estimated 20–80% edge width as follows:

$$d_x(\text{Edge}) = \frac{0.22\lambda}{na\cos\theta}, \quad (5)$$

or an edge width of 0.75 μm from Eq. (5), with a N.A. of 0.165. Figure 3(b) shows the response to the chrome surface taken in the axial direction with a FWHM of 2.1 μm, which should be compared to the estimated value of 2.2 μm from Eq. (3).

Reflectance images were collected from fresh biopsy specimens of normal human esophagus, a tissue accessible by endoscopy. Informed consent was obtained from the patient before the routine procedure. Specimens approximately 1 mm^3 in size were resected with biopsy forceps, and the mucosal surface was oriented normal to the midline axis. Approximately 1 ml of 6% acetic acid was applied to enhance contrast.[7] After image acquisition, the specimens were evaluated by routine histology. Figure 4 shows an image in a FOV of 200 μm at a depth of 10 μm; the scale bar is 20 μm. The cell nuclei (arrows) and membrane (arrowhead) can be clearly distinguished. These structures were confirmed by direct comparison with histology. We used the Adobe Photoshop 6.0 program to determine the average areas of the nucleus and of the cytoplasm of 12 epithelial cells and found them to be 71 ± 16 μm^2 and 1000 ± 290 μm^2, respectively, resulting in an average nuclear-to-cytoplasm ratio of 0.07 ± 0.02. These values are comparable to those measured from the corresponding histology sections.

The dual-axes design demonstrates several advantages over the single-axis design for purposes of miniaturization and *in vivo* imaging. First, sub-cellular resolution can be achieved easily in the axial as well as in the transverse dimension. Second, low-N.A. lenses that we use are relatively less sensitive to aberrations and are easy to fabricate with small dimensions. Third, a long WD is created that allows for a miniature mirror to be placed on the focused beam side of the objective to provide a large FOV. Fourth, light scattered along the illumination path outside the focal volume is less likely to be collected, thus enhancing detection sensitivity and dynamic range. The multiple scattering events required for the returning photons that originate outside the focal volume to arrive at the proper trajectory for detection occur with low probability. Finally, this method of imaging, unlike optical coherence tomography, can be used for collection of noncoherent light such as fluorescence.

In conclusion, we have presented a novel confocal microscope design that uses two low-N.A. lenses oriented in a dual-axes configuration and demonstrated sub-cellular transverse and axial resolution, long working distance, and large field of view. We have confirmed subcellular resolution is freshly resected human tissue. The illumination and collection optics are fiber coupled and scalable to millimeter dimensions. Future development of this microscope involves miniaturization with MEMS fabrication techniques followed by *in vivo* medical and biological imaging with reflectance and fluorescence.

Acknowledgements

We thank Mark H. Garrett and Matthew P. Scott for insightful discussions and George Triadafilopoulos for his technical assistance. This research was supported, in part, by grants from the National Institutes of Health including T32DK07056-27 (T. D. Wang), 1 R43 GM64028-01" (M. J. Mandella), CA88303, CA92862, and CA86312 (C. H. Contag), and unrestricted gifts from the Bio-X program at Stanford University and the Johnson Center for Perinatal Research as part of the Lucille Packard Foundation's Child Health Initiative. T. D. Wang's e-mail address is tdwang@stanford.edu.

References

1. Pawley, J., editor. Handbook of Biological Confocal Microscopy. 3. Plenum; New York: 1996.
2. Corle, TR.; Kino, GS. Confocal Scanning Optical Microscopy and Related Imaging Systems. Academic; Boston, Mass.: 1996.
3. Rajadhyaksha M, Anderson RR, Webb RH. Appl Opt 1999;38:2105.
4. Dickensheets DL, Kino GS. Opt Lett 1996;21:764.
5. Webb RH, Rogomentich F. Appl Opt 1999;38:4870.
6. Stelzer EHK, Lindek S. Opt Commun 1994;111:536.
7. Zuluaga AF, Drezek R, Collier T, Lotan R, Follen M, Richards-Kortum R. J Biomed Opt 2002;7:398. [PubMed: 12175289]

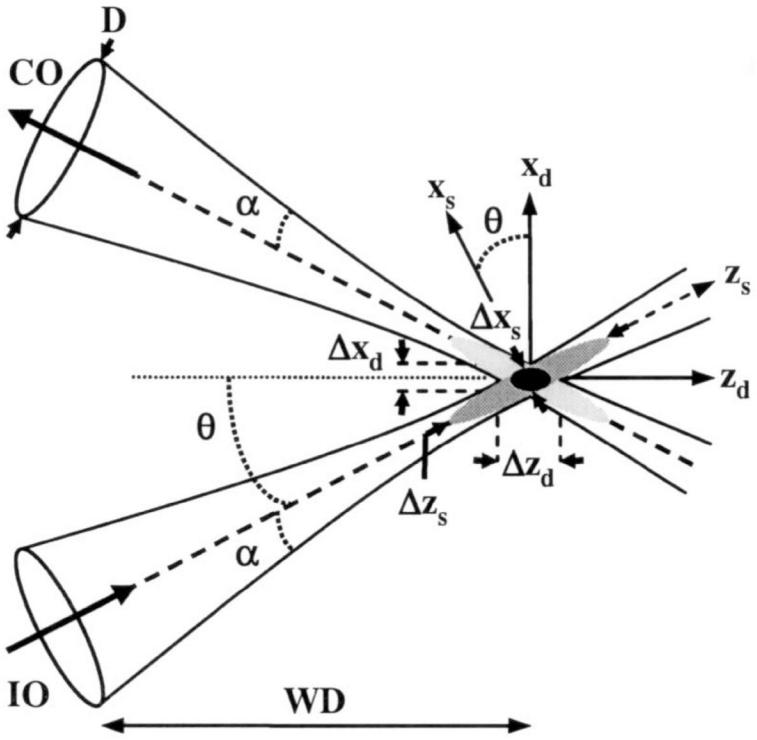

Fig. 1.
Schematic diagram of the dual-axes design: *D*, lens diameter; other notation defined in text.

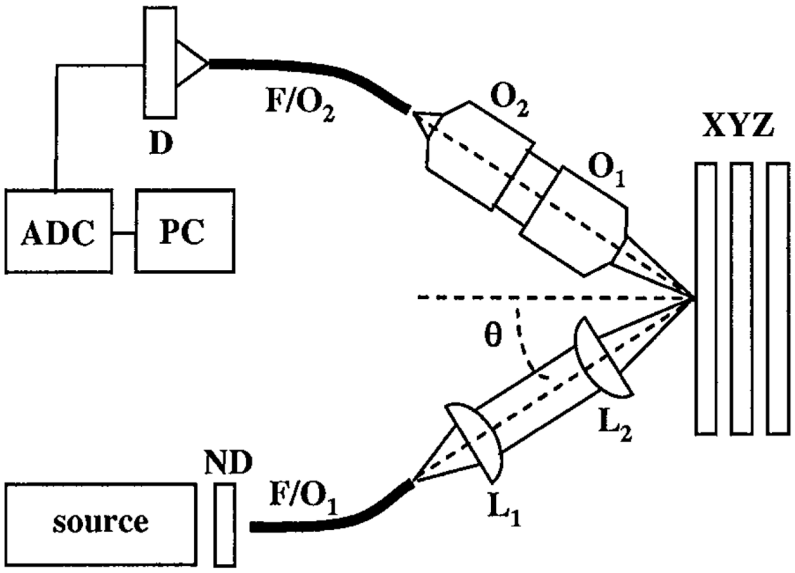

Fig. 2.
Schematic of the optical setup: D, detector; ADC, analog-to-digital converter; PC, personal computer; other abbreviations defined in text.

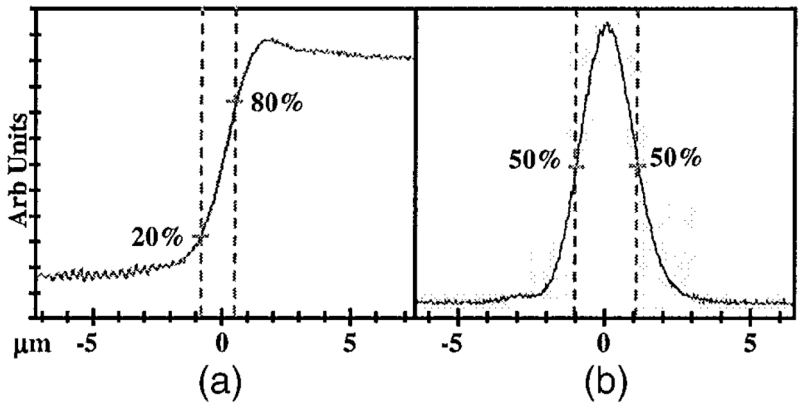

Fig. 3.

(a) Transverse response to chrome edge; measured 20–80% width, 1.06 μm. (b) Axial response to chrome; measured FWHM spot length, 2.1 μm.

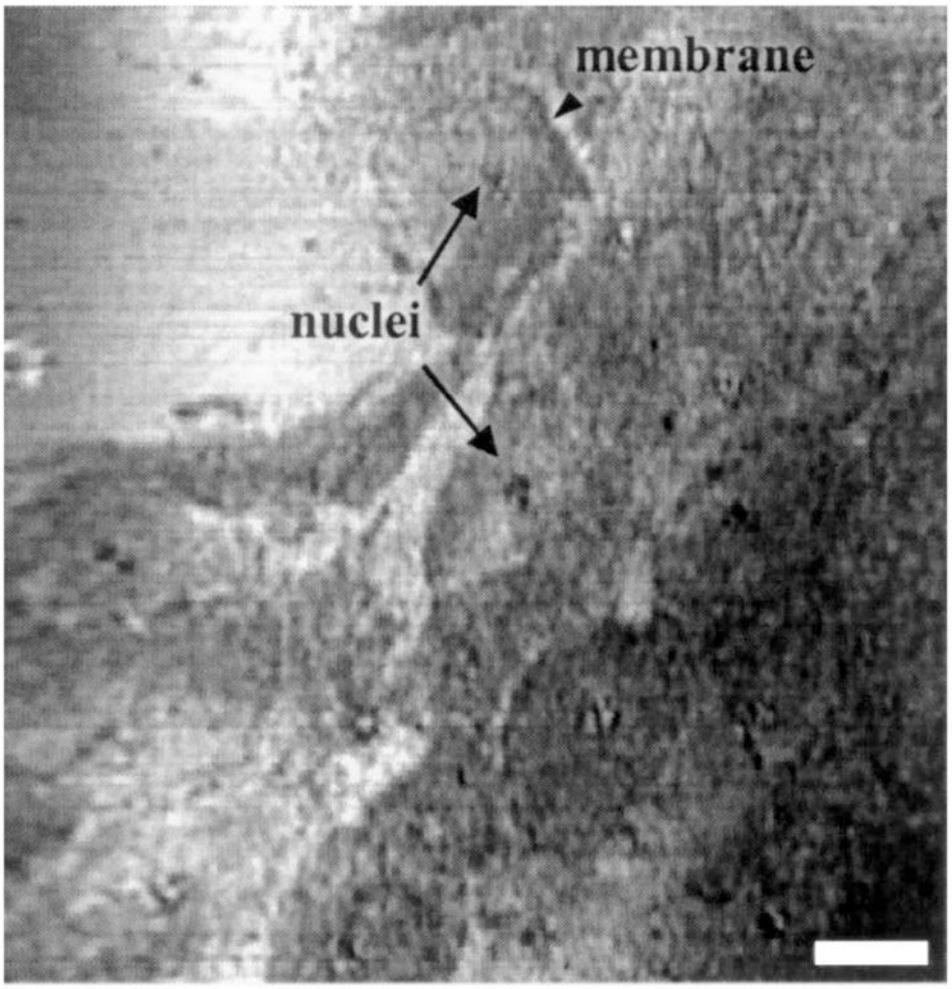

Fig. 4.
This reflectance image of normal esophageal mucosa collected *ex vivo* reveals cell nuclei and membrane; scale bar, 20 μm.